Computer Aided Surgery, Month 2004; 9(5/6): 1–9

Taylor & Francis
healthsciences

BIOMEDICAL PAPER

Virtual Remote Center of Motion control for needle-placement robots

EMAD M. BOCTOR[1,3], ROBERT J. WEBSTER III[1,2], HERVE MATHIEU[1], ALLISON M. OKAMURA[1,2], & GABOR FICHTINGER[1,3]

[1]*Engineering Research Center for Computer Integrated Surgical Systems and Technology,* [2]*Department of Mechanical Engineering, and* [3]*Department of Computer Science, Johns Hopkins University, Baltimore, Maryland*

Abstract

Objective: We present an algorithm that enables percutaneous needle-placement procedures to be performed with unencoded, unregistered, minimally calibrated robots while removing the constraint of placing the needle tip on a mechanically enforced Remote Center of Motion (RCM).

Materials and Methods: The algorithm requires only online tracking of the surgical tool and a five-degree-of-freedom (5-DOF) robot comprising three prismatic DOF and two rotational DOF. An incremental adaptive motion control cycle guides the needle to the insertion point and also orients it to align with the target-entry-point line. The robot executes RCM motion without having a physically constrained fulcrum point.

Results: The proof-of-concept prototype system achieved 0.78 mm translation accuracy and 1.4° rotational accuracy (this is within the tracker accuracy) within 17 iterative steps (0.5–1 s).

Conclusion: This research enables robotic assistant systems for image-guided percutaneous procedures to be prototyped/constructed more quickly and less expensively than has been previously possible. Since the clinical utility of such systems is clear and has been demonstrated in the literature, our work may help promote widespread clinical adoption of this technology by lowering system cost and complexity.

Keywords: *Needle insertion, visual feedback, image guidance, medical robotics*

Key link: http://www.cisst.org

Introduction

Recent advances in medical imaging have induced a rapid increase in minimally invasive image-guided interventions, such as biopsy and needle-based local therapies. The success of these procedures hinges on the accuracy of needle placement. Conventional unassisted freehand techniques depend primarily on the physician's hand-eye coordination and thus often suffer from inaccuracy and inconsistency in needle placement. As an appealing alternative, medical robots offer the potential to manipulate surgical instruments more precisely and consistently than is possible by hand. At the same time, however, contemporary medical robots introduce a prohibitively complex engineering entourage into otherwise rather straightforward needle-placement procedures.

Manual needle placement typically includes the following three decoupled tasks: (1) moving the needle tip to the pre-selected entry point with 3-DOF Cartesian motion; (2) orienting the needle by pivoting around the entry point using 2-DOF rotation; and (3) inserting the needle into the body using 1-DOF translation along a straight trajectory. The technical challenge for robot-assisted needle placement has been to reproduce this sequence of motions robotically in a safe, practical and affordable manner.

Correspondence: Gabor Fichtinger/Emad Boctor, Department of Computer Science, Johns Hopkins University, 3400 N. Charles St., Baltimore, MD 21218. Tel: 410-516-3417. Fax: 410-516-5553. E-mail: gabor@cs.jhu.edu or eboctor@ieee.org

This paper is based on research presented at the 6th International Conference on Medical Image Computing and Computer-Assisted Intervention (MICCAI), Montreal, Canada, November, 2003.

ISSN 1092-9088 print/ISSN 1097-0150 online
DOI: 10.1080/10929080500097661

One possibility is to use serial linkages and coordinate the joints mathematically under computer control, as is done in the commercial Zeus™ and Aesop™ laparoscopic robots (Intuitive Surgical, Inc., Mountain View, CA). Similar solutions were used in the IGOR [1], PUMA [2,3], Neuromate [4,5], Kawasaki [6] and Sankyo Scara [7] robots. However, serial linkages present two fundamental problems. First, the robot kinematics induce mathematical singularities in the active workspace, which is prohibitive in most medical applications. Another difficulty with conventional serial robots is the need for a fully described and precisely encoded kinematic chain. It is rather difficult to calibrate these arms, and losing calibration accuracy during clinical use is a critical risk. Their trajectory and range of motion is controlled solely by software, which increases the operative risks of these devices.

A decidedly more appealing and safer alternative is the family of kinematically decoupled robots. These devices contain separately controlled and sequentially operated Cartesian, rotational and insertion stages, and they thus appear to be a more natural fit for the process of needle placement. They are also safer, because the range of motion of each individual stage can be independently constrained and, if necessary, mechanically blocked, thereby preventing overdriving of any individual axis. The least straightforward action for a decoupled needle-placement robot is orienting the needle toward the pre-selected target. One approach is to use a 2-DOF design that mechanically constrains the fulcrum point at the needle tip. For this function, goniometric arcs have been proposed [8], but these are impractical for needle placement because the fulcrum point has to be in the center of the arcs, thereby blocking access to the patient. Taylor and colleagues implemented the remote center of motion (RCM) point concept in a laparoscopic robot [9], where the fixed fulcrum point is produced farther away from the mechanism, thereby leaving room for surgical instruments and allowing the physician access to the patient. The RCM concept has been applied in several laparoscopic and needle-placement robots, including commercial systems such as the da Vinci™ (Intuitive Surgical, Inc.). At Johns Hopkins University, Stoianovici et al. developed a chain-drive RCM robot that is used in conjunction with a radiolucent needle driver for percutaneous access [10]. Variants of this robot have been tested under image guidance using fluoroscopy [11], computed tomography (CT) [12], ultrasound [13] and CT-fluoroscopy [14]. The workflow in these systems is usually as follows: (1) register robot to imager; (2) select target and entry points; (3) solve inverse kinematics; (4) move needle to entry; (5) line up needle with target; and (6) insert needle. Depending on the number of actuated degrees of freedom available, some steps may be executed manually, but the workflow remains the same. While the RCM paradigm has made significant impact on the field, it also has some disadvantages: (1) precise construction must guarantee the existence of a known fulcrum point; (2) a tool holder must be carefully designed for each new tool, placing it exactly on this fulcrum point; (3) each joint must be fully encoded; and (4) the kinematic chain must be known *a priori*. The net result of these factors is usually a complex and expensive structure that must be carefully designed, manufactured and calibrated.

An appealing alternative to the mechanically constrained fulcrum point would be to generate a programmed or "virtual" RCM in software, while still taking advantage of decoupled and uncalibrated Cartesian, rotational and insertion stages. This problem is the focus of our research.

Contemporary MRI, fluoroscopy and CT-fluoroscopy allow real-time visualization, which enables real-time tracking of surgical instruments. Three-dimensional ultrasound-guided interventional systems [13,15] also include a real-time tracker in the field of interest. In these systems, one can track the end-effector of a surgical robot and manipulate the device under visual servo control. It has been known in general robotics that the operational space formulation [16] and partitioned control [17] can be used to alter the behavior of the system so that it appears, kinematically and dynamically, to be an RCM device. Unfortunately, existing kinematic and dynamic models need to be precise, so the joints must be fully encoded and calibrated. Extensive research has also been devoted to visual servo control [18], but work applied to uncalibrated and/or unencoded robots has focused on estimating the robot's Jacobian rather than generating a virtual Remote Center of Motion (Virtual RCM). Artificial intelligence-based algorithms for robot motion have also been investigated but not yet applied to the needle-placement task. These algorithms have been used in the control of uncalibrated mobile robots to explore unknown environments and navigate familiar environments [19]. Related research has also examined the effect of uncertainty in robot sensors and/or the environment [20] in generating a collision-free map of the space.

Our present contribution combines an uncalibrated needle-placement robot from three linear, two rotational, and one linear insertion stages and an AI-based motion algorithm to create a Virtual RCM robot that requires neither encoded joints nor complete knowledge of the robot kinematics. Unlike classic RCM robots, the Virtual RCM method does not require (1) the existence of a physically fixed fulcrum point, (2) *a priori* knowledge of

the kinematic chain, or (3) encoding of the joints. This relaxes many requirements previously imposed on RCM needle-placement robots. For example, the axes of the prismatic stages need not be orthogonal; the axes of rotation stages need not intersect; and kinematically unknown passive linkages are permitted anywhere within the chain. This allows robots using the Virtual RCM algorithm to be simple and inexpensive to construct, eliminates laborious calibration, and permits testing of new robots or parts of robots to proceed rapidly without affecting the accuracy of image guidance.

Materials and methods

System overview

Our proof-of-concept system (Figure 1) is comprised of a 3-DOF motorized Cartesian stage (NEAT, Inc.), a passive unencoded adjustable arm, and a 2-DOF motorized rotational stage designed by Stoianovici et al. [10]. The Virtual RCM algorithm requires measurement of the pose of a point on the robot with a known transformation to the tool frame. In clinical practice, fiducials attached to the robot can provide this information directly from CT [21] or MRI images. When using ultrasound (US) as the imaging modality, magnetic tracking can provide the pose of both the image and the tool [22]. In our system, we attach a magnetic tracker to the tool holder (Flock of Birds, model 6D FOB, Ascension Technology Corporation, Burlington, VT). The passive arm shown in Figure 1 helps in gross initial positioning of the needle tip and also purposely introduces an unknown linkage in the kinematic chain, demonstrating that the Virtual RCM does not require known kinematics. The tool holder also purposely removes the RCM property of the Stoianovici rotation stage by holding the needle off the RCM point, demonstrating that the Virtual RCM does not require careful construction of the fulcrum constraining mechanism or the tool holder.

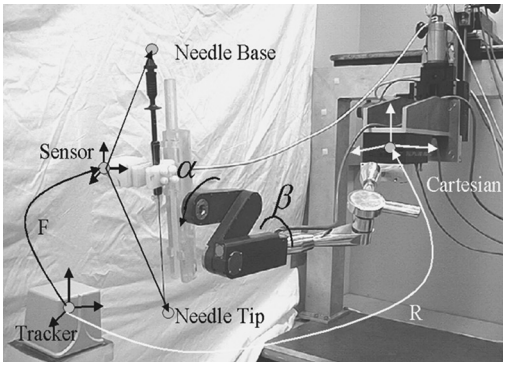

Figure 1. Experimental setup.

Low-level control of the robot is achieved using a motion control card (MEI, Inc., Santa Barbara, CA), driven with the Modular Robot Control (MRC) library developed at Johns Hopkins University [23]. The readings of the FOB tracker are reported to a PC running the 3D Slicer medical data visualization package [24]. Slicer is a public domain open-source program primarily developed by the MIT AI Lab and the Surgical Planning Laboratory at the Brigham and Women Hospital, with sustained contribution from Johns Hopkins University. In Slicer, we create a 3D virtual environment (Figure 2) in which objects are represented in the FOB tracker coordinate frame.

The incremental adaptive motion cycle of the Virtual RCM algorithm that aligns and translates the needle (as verified experimentally in the *Experimental implementation* section below) requires the transformation between the magnetic sensor and the tool frame. Using readings from the FOB tracker, this transformation is determined off-line by a version of the pivot calibration [25]. Also required is the orientation of the Cartesian stage expressed in the coordinate frame of the tracker. This is obtained by moving the Cartesian stage arbitrarily (maintaining a safe distance from the patient) while recording sensor readings. Direction cosines yield the orientation of the Cartesian stages with respect to the tracker.

The Virtual RCM: a heuristic search

In addition to accuracy and robustness, a key performance criterion for the Virtual RCM needle-placement algorithm is fast convergence within very few cycles. In systems where the Virtual RCM algorithm is implemented (where the tool tip is not mechanically constrained to an RCM point), the roll and pitch DOF (α and β) are no longer decoupled and thus cannot be optimized individually. A blind search of all possible α and β combinations is not useful for these coupled variables, because it would be impractical to repeatedly rotate the two joints through a full 360° until the best alignment was determined from all possible discrete combinations of the two variables. To rapidly optimize these two variables simultaneously, we draw upon artificial intelligence techniques, such as a heuristic-based Breadth First Search (BFS) or Depth First Search (DFS). We discretize each rotational DOF and partition our search space into two subspaces, one for each angle. A heuristic function rapidly guides the search to optimal needle alignment by deciding where to search next at each state.

In practical terms, this means that the robot makes incremental motions, and after each motion uses the heuristic function to observe whether the needle is becoming more or less aligned. This enables the

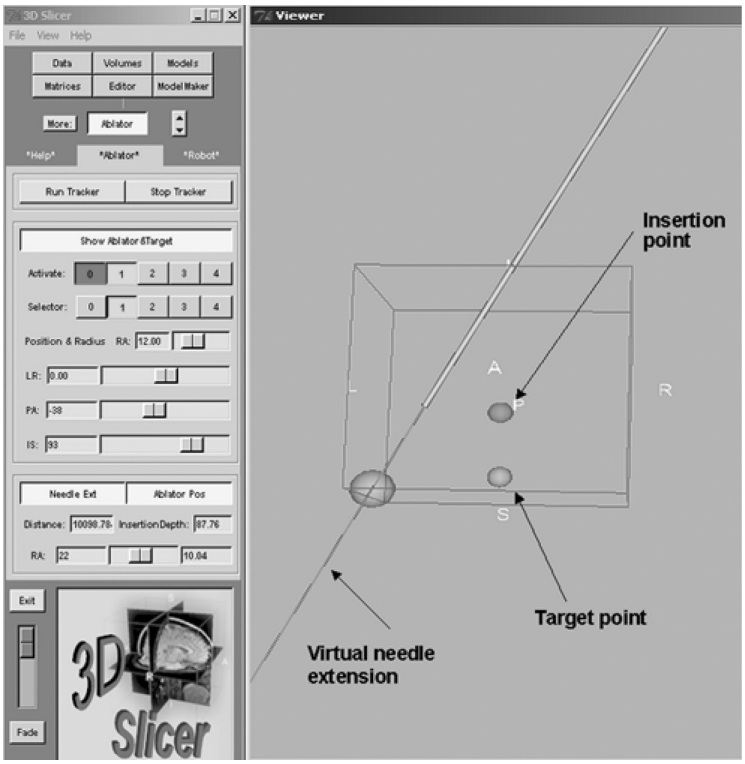

Figure 2. Slicer graphical user interface.

algorithm to determine which direction of motion is likely to cause better alignment. By continually moving both angles, the robot is able to rapidly home in on the proper alignment.

Selecting a heuristic function that quantifies improvement in needle alignment is not trivial. A desirable function would not have local minima that may cause the final alignment to converge at an incorrect solution. Another consideration is that the magnetic tracker (or any device that provides the pose of the needle) introduces some uncertainty. Therefore, a good heuristic function must have a low sensitivity to noise, and it is important to conduct an error propagation analysis of candidate heuristic functions. This can be done by applying Equation 1 (below), where z represents a heuristic function measure. The quantity z is a function of measurements, denoted by x and y, subject to sensor uncertainty. The standard deviations (σ_x and σ_y) represent the uncertainties in measurement. The total uncertainty of the heuristic function z is then given by:

$$\sigma_z^2 = \frac{\partial f(x,y)}{\partial x}\sigma_x^2 + \frac{\partial f(x,y)}{\partial y}\sigma_y^2 \qquad (1)$$

This indicates that heuristic functions where sensor readings are multiplied/divided are much more sensitive to sensor noise than heuristic functions that involve only addition and subtraction.

Analysis of candidate heuristic functions

One potential heuristic function is the cross-product between the needle vector and the entry path vector. The needle vector is defined from the needle base to the needle tip and the entry path as the vector from the entry point to the target position. Minimizing the magnitude of the cross-product between these two vectors yields a needle aligned with the entry path.

Another potential heuristic function to move and align the needle is to first minimize the distance between the needle tip and the entry point (d in Figure 3), and then align the needle by minimizing d_{normal} while maintaining the needle tip at the entry point. We will see in simulation that each of these is a poor candidate heuristic function because they have local minima that can cause the needle to become misaligned.

To compare different heuristic functions, we build a simulator reflecting our robot configuration. As shown in Figure 4, we have an RCM frame at the RCM point and two rotational DOF (α and β around the x and y axes, respectively). We also have a tracker frame, where the planned "entry" and "target" points are defined. Most importantly, the transformation between these two frames is $F_{rcm}^{tracker}$,

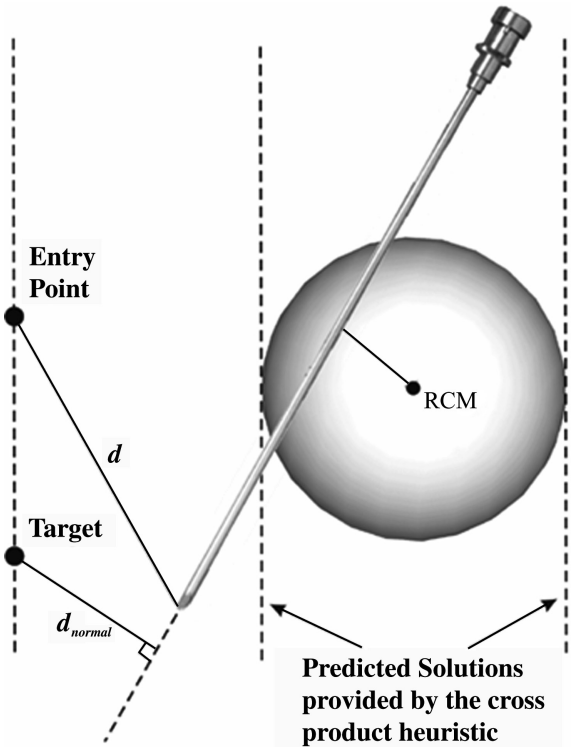

Figure 3. Heuristic functions.

which is not required in the physical system (no calibration step is necessary), but is assigned a value for simulation purposes. The needle coordinates in the RCM frame (note: the needle tip is not at the RCM point) can be transformed to the tracker frame as follows:

$$\vec{n}_{tip}^{\,trac\,ker} = F_{rcm}^{trac\,ker} R(\vec{x}, \alpha) R(\vec{y}, \beta) \vec{n}_{tip}^{\,rcm}$$
$$\vec{n}_{base}^{\,trac\,ker} = F_{rcm}^{trac\,ker} R(\vec{x}, \alpha) R(\vec{y}, \beta) \vec{n}_{base}^{\,rcm}$$

where $R(\vec{x}, \alpha)$ is a rotation around the x-axis by α degrees, and $R(\vec{y}, \beta)$ is a rotation around the y-axis by β degrees. Now, we have the needle base and tip points in the tracker space where the planned entry-target points are defined. The following will illustrate the different heuristic functions that were simulated to check the applicability of each one:

$$cross - product = \left\| (\vec{n}_{base}^{\,trac\,ker} - \vec{n}_{tip}^{\,trac\,ker}) \times (\vec{p}_{entry}^{\,trac\,ker} - (\vec{p}_{t\,arg\,et}^{\,trac\,ker} \right\|$$
$$dist.metric = dist(\vec{n}_{base}^{\,trac\,ker}, \vec{n}_{tip}^{\,trac\,ker}, \vec{p}_{entry}^{\,trac\,ker}, \vec{p}_{t\,arg\,et}^{\,trac\,ker})$$

Comparing the distance heuristic function with the cross-product heuristic function illustrates why the cross-product is the preferred choice for creating a Virtual RCM. The distance heuristic function requires the needle tip to be placed at the insertion point, while the cross-product heuristic function search can take place with the needle anywhere in space. The cross-product will also be subject to less alignment error, as illustrated by the simulation in the next section.

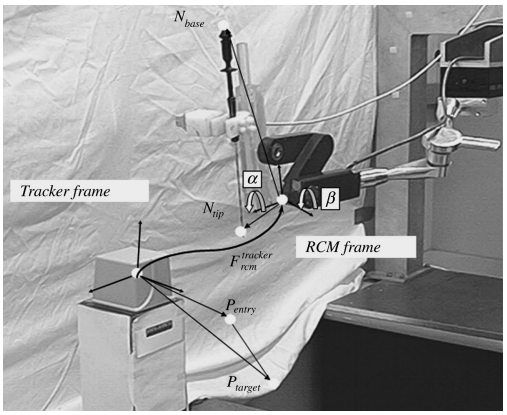

Figure 4. Illustration of frames and vectors necessary for building a simulation of candidate heuristic functions.

Simulation results

In simulation, all possible discrete combinations of α and β can be plotted with respect to the scalar value of a given heuristic function. This yields visual and intuitive understanding of the heuristic functions. Figure 5 shows the simulated needle as α is rotated through a full 360° while β is held constant at 5° and 50°. This procedure is repeated for each β value. Plots of two heuristic function results across the entire α-β space can be seen in Figure 6. As can be seen from this figure, the cross-product heuristic function has a higher specificity than alternative heuristic functions. Its deep minima will yield a more accurate alignment result in the presence of sensor noise or other real-world uncertainties than the shallow minima of the distance heuristic function.

At first glance, it may not be obvious which of the minima on the cross-product are acceptable solutions. Two of the four minima can be discarded immediately, because they represent the needle being oriented the wrong way, with its base toward the target. The other two minima are equally good solutions, representing the needle being aligned on either side of the actual RCM point, as shown by the dashed lines on Figure 3. The only potential reason for choosing one over the other would be application-specific workspace constraints, since both represent equally good alignments of the needle. If no such workspace constraints exist, this interesting multiple solution property of the cross-product heuristic function is beneficial to the speed of the algorithm. A search of a multiple-solution

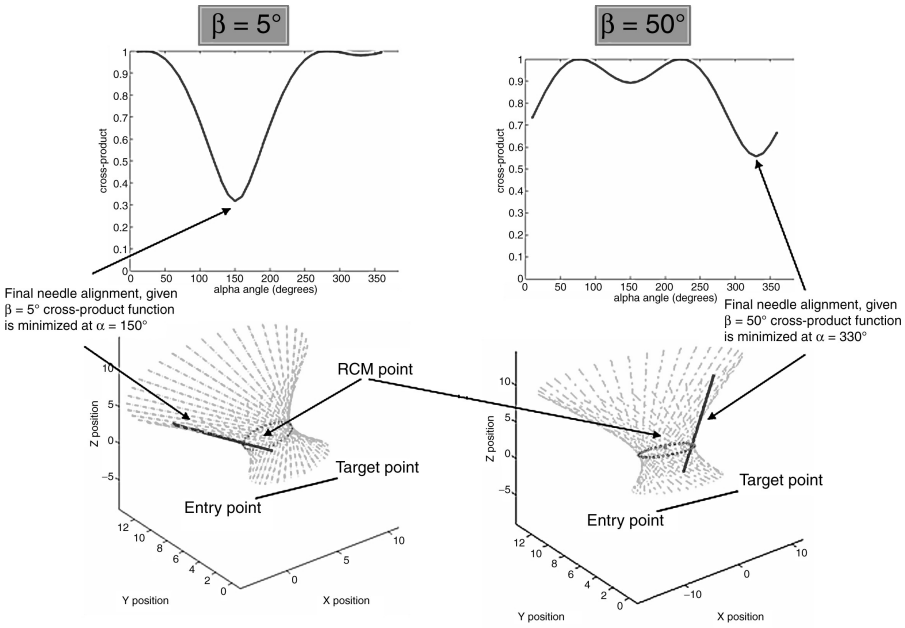

Figure 5. This shows 360 rotations of α for two particular β angles to show the dependency between α and β. Note: alignment is better on the left as shown in the cross-product value 0.3, while on the right the cross-product value is 0.55.

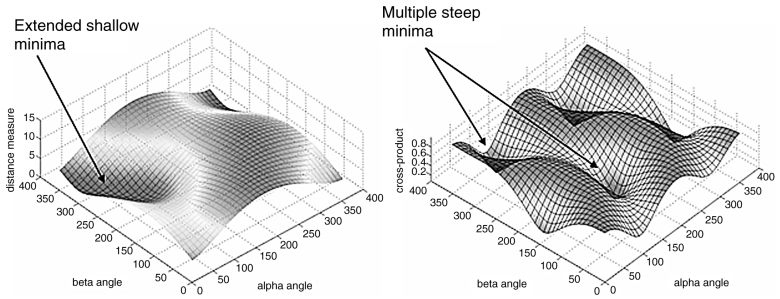

Figure 6. Plot of distance (left) and the cross-product (right) heuristic functions for all angular values.

space can generally converge more quickly than a search with a single solution.

The most compelling advantages of the cross-product are its spatial invariance and its low overall error in alignment. The magnitude of a spatially invariant function does not change with Cartesian motion. This has important practical implications for patient safety, as described in the next section. Even more important to practical application, the cross-product will have lower final error than the distance heuristic function, because the former requires only summation of error, while the latter requires both multiplication and square root functions.

Experimental implementation

The two rotational joints of the robot perform needle alignment using the cross-product heuristic function described previously. The joints are moved in small increments. Since the tool tip is not on the mechanical fulcrum point, it will be displaced a small amount during each rotation. However, this displacement is immediately compensated for by the Cartesian stages, based on the tracker reading. Thus, the needle tip remains on a Virtual RCM point. The robot continues to move through the search tree by moving the rotational joints alternately in incremental motions that decrease the value of the heuristic function.

There are several ways to apply this algorithm in needle placement (Figure 7). The most obvious is to perform needle placement using the same sequence of motions as would be done manually (the Virtual RCM Method), where the robot first moves the needle tip to the entry location, then aligns it along the insertion vector. Humans do not orient the needle first and then move it to the entry point, although this is an equally good order of operations. (Perhaps the reason is that humans are able to discern smaller differences in vector alignment

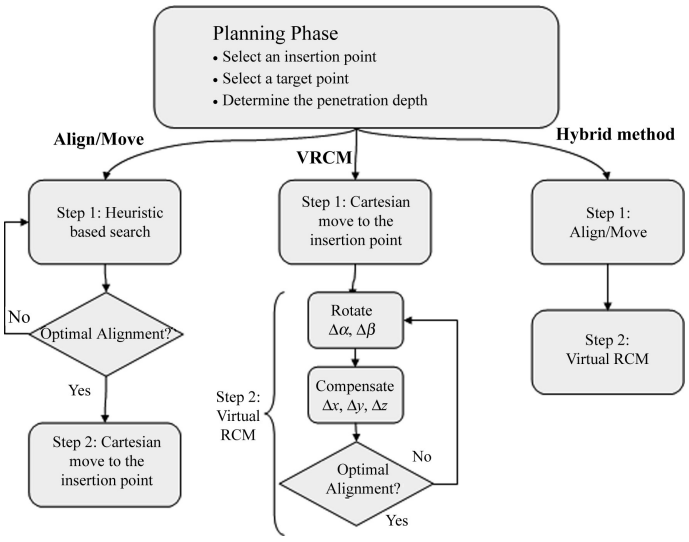

Figure 7. Needle insertion scenarios flow chart.

between nearby vectors than between those separated by a distance of many centimeters. It may also be easier for humans to control the alignment more accurately by pivoting the needle on a fixed point.)

Since robots suffer from no such limitations, there is no intrinsic reason why a robot could not perform alignment before moving the needle to the surgical site (the Align/Move Method). The advantage of this for the robot is speed: Since the robot is at a safe distance from the patient, we can eliminate the use of the Cartesian correction portion of the Virtual RCM algorithm and find the correct alignment more rapidly.

A third alternative is to use a combination of the first two methods (the Hybrid Method). The robot can rapidly make a quick rough alignment of the needle away from the patient, and then move to the insertion point (Align/Move Method) and finally fine-tune the alignment with Virtual RCM motion (Virtual RCM Method). Figure 7 presents a flow chart of all three methods: Align/Move, Virtual RCM and Hybrid.

Results and discussion

We performed needle placement according to each of the three methods, and the results are summarized in Table I. In our experiment, the number of steps required (regardless of the method used) was nearly linearly proportional to the initial misalignment.

Table I. Experimental results.

Method	Experiment sets	Set I	Set II	Set III
	Initial angle deviation (°)	15.6	28.7	51.4
	Initial target displacement (mm)	21.2	41.8	118.2
Align/Move	No. of steps			
	Rotation	17	35	66
	Translation	1	1	1
	Angle error (°)	**2.2**	**2.8**	**2.1**
	Target displacement (mm)	1.05	2.81	3.40
Virtual RCM	No. of steps			
	Rotation	17	35	66
	Translation	17	35	66
	Angle error (°)	**2.8**	**2.2**	**2.8**
	Target displacement (mm)	1.68	3.02	5.15
Hybrid Tech.	No. of steps			
	Rotation			
	Method I	17	35	66
	Method II	2	2	3
	Translation	2	2	3
	Angle error (°)	**1.4**	**1.7**	**1.9**
	Target displacement (mm)	0.78	2.44	3.99

This was because a fixed initial (largest) step size was used. If the initial step size were large and adaptively modified as the solution was approached, the algorithm could reach a solution in fewer steps. However, this would only be practically feasible for safety reasons in the Align/Move or Hybrid Methods, where the needle tip is away from the patient or the alignment is already nearly correct. In our experiments it was possible, given a wide range of initial conditions, to obtain an optimized solution within a few (20–30) steps, requiring a total time of only 0.8–1.2 s, since each step takes an average of 40 ms.

As can be seen from Table I, Align/Move is the fastest (requiring the fewest steps) of the three methods, because no Cartesian motion is needed to compensate for tip displacement. The results for Virtual RCM show that it alone is essentially equivalent to Align/Move in both rotational and displacement accuracy, but is much slower. The Hybrid method is much more accurate than the first two, yet the algorithmic complexity has the same order of magnitude as Align/Move. It is important to note that the accuracy presented in the table is severely limited by the tracker accuracy, which is reported by the manufacturer as 2.54 mm RMS (this is a first-generation FOB tracker).

A future goal is to replace the magnetic tracker with a CT-fluoroscopy (CTF) scanner. We will gather the pose of the needle tip directly from the CTF images using the method described in reference [21]. Our ultimate goal is to clinically accurately place needles using inexpensive, uncalibrated, and unencoded robots in intra-operative imagers (CTF, MRI, and X-ray fluoroscopy), with the use of purely image-based spatial registration of the tool holder alone. We also hope to perform experiments under ultrasound guidance, where the external tracker will be retained. In terms of algorithmic enhancements, we will incorporate target uncertainty into our model to account for motion artifacts.

Acknowledgments

The authors acknowledge the support of the NSF under the Engineering Research Center grant #EEC-9731478 and a National Defense Science and Engineering Graduate Fellowship supporting Robert Webster. We thank Prof. Russell Taylor for his comments and Dr. Dan Stoianovici for access to and maintenance of the RCM mechanism.

References

1. Cinquin P, Troccaz T, Demongeot J, Lavallee S, Champleboux G, Brunie L, Leitner F, Sautot P, Mazier B, Perez A, Djaid M, Fortin T, Chenic M, Chapel A. IGOR: Image Guided Operating Robot. Innovation et Technol Biol Med 1992;13:374–94.
2. Davies BL, Hibberd RD, Ng WS, Timoney AG, Wickham JE. The development of a surgeon robot for prostatectomies. Proc Inst Mech Eng 1991;205(1):35–8.
3. Kwoh YS, Hou J, Jonckheere EA, Hayati S. A robot with improved absolute positioning accuracy for CT guided stereotactic brain surgery. IEEE Trans Biomed Eng 1988; 35(2):153–60.
4. Varma TR, Eldridge PR, Forster A, Fox S, Fletcher N, Steiger M, Littlechild P, Byrne P, Sinnott A, Tyler K, Flintham S. Use of the NeuroMate stereotactic robot in a frameless mode for movement disorder surgery. Stereotact Funct Neurosurg 2003;80(1–4):132–5.
5. Li QH, Zamorano L, Pandya A, Perez R, Gong J, Diaz F. The application accuracy of the NeuroMate robot – a quantitative comparison with frameless and frame-based surgical localization systems. Comput Aided Surg 2002;7(2):90–8.
6. Yanof J, Haaga J, Klahr P, Bauer C, Nakamoto D, Chaturvedi A, Bruce R. CT-integrated robot for interventional procedures: preliminary experiment and computer–human interfaces. Comput Aided Surg 2001;6(6):352–9.
7. Rovetta A. Tests on reliability of a prostate biopsy telerobotic system. Stud Health Technol Inform 1999;62: 302–7.
8. Harris SJ, Arambula-Cosio F, Mei Q, Hibberd RD, Davies BL, Wickham JE, Nathan MS, Kundu B. The Probot – an active robot for prostate resection. Proc Inst Mech Eng 1997;211(4):317–25.
9. Taylor RH, Funda J, Eldridge B, Gruben K, LaRose D, Gomory S, Talamini M, Kavoussi LA, Anderson JH. A telerobotic assistant for laparoscopic surgery. IEEE EMBS Magazine: Special Issue on Robotics in Surgery. 1995. p 279–91.
10. Stoianovici D. URobotics – Urology Robotics at Johns Hopkins. Comput Aided Surg 2001;(6):360–9.
11. Su LM, Stoianovici D, Jarrett TW, Patriciu A, Roberts WW, Cadeddu JA, Ramakumar S, Solomon SB, Kavoussi LR. Robotic percutaneous access to the kidney: comparison with standard manual access. J Endourol 2002;16(7):471–5.
12. Fichtinger G, DeWeese TL, Patriciu A, Tanacs A, Mazilu D, Anderson JH, Masamune K, Taylor RH, Stoianovici D. System for robotically assisted prostate biopsy and therapy with intraoperative CT guidance. Acad Radiol 2002;9(1): 60–74.
13. Boctor EM, Fischer G, Choti M, Fichtinger G, Taylor R. Dual-armed robotic system for intraoperative ultrasound guided hepatic ablative therapy: a prospective study. In: Proceedings of 2004 IEEE International Conference on Robotics and Automation (ICRA'04), New Orleans, LA, April 26–May 1, 2004. p 2517–22.
14. Solomon SB, Patriciu A, Bohlman ME, Kavoussi LR, Stoianovici D. Robotically driven interventions: a method of using CT fluoroscopy without radiation exposure to the physician. Radiology 2002;225(1):277–82.
15. Wei Z, Wan G, Gardi L, Mills GR, Downey DB, Fenster A. Robot-assisted 3D-TRUS guided prostate brachytherapy: system integration and validation. Med Phys 2004;31(3): 539–48.
16. Khatib O. A unified approach for motion and force control of robot manipulators: The Operational Space Formulation. IEEE J Robotics Automation 1987;RA-3(1):43–53.
17. Craig JJ. Introduction to Robotics Mechanics and Control. Third Edition. Reading, MA: Addison Wesley, 1992.
18. Hutchinson S, Hager GD, Corke P. A tutorial introduction to visual servo control. IEEE Trans Robotics Automation 1996;12(5):651–70.
19. Donald BR. A search algorithm for motion planning with six degrees of freedom. Artificial Intelligence 1987;(31): 295–353.

20. Betke M. Learning and Vision Algorithms for Robot Navigation. PhD dissertation, Massachusetts Institute of Technology, June 1995.
21. Lee S, Fichtinger G, Chirikjian GS. Novel algorithms for robust registration of fiducials in CT and MRI. J Med Physics 2002;29(8):1881–91.
22. Boctor EM, Webster RJ, Choti MA, Taylor RH, Fichtinger G. Robotically assisted ablative treatment guided by freehand 3D ultrasound. In: Lemke HU, Vannier MW, Inamura K, Farman AG, Doi K, Reiber JHC, editors. Computer Assisted Radiology and Surgery. Proceedings of the 18th International Congress and Exhibition (CARS 2004), Chicago, IL, June 2004. Amsterdam: Elsevier, 2004. p 503–8.
23. Taylor RH, Kumar R et al. Library of Modular Robots Control. Engineering Research Center Computer Integrated Surgical Systems and Technology (ERC-CISST). http://www.cisst.org/resources/software/mrc/
24. Kikinis R et al. 3D Slicer: Medical Visualization and Processing Environment for Research. MIT Artificial Intelligence Lab and the Surgical Planning Lab at Brigham & Women's Hospital. http://www.slicer.org/
25. Boctor EM, Fichtinger G, Taylor RH, Choti MA. Tracked 3D ultrasound in radio-frequency liver ablation. In: Walker WF, Insana MF, editors. Proceedings of SPIE Medical Imaging 2003: Ultrasonic Imaging and Signal Processing. Proc SPIE 2003;5035:174–82.